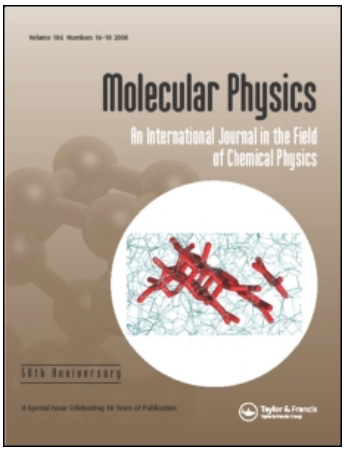

Molecular Physics
Publication details, including instructions for authors and subscription information:
http://www.informaworld.com/smpp/title~content=t713395160

A new determination of the ground state interatomic potential for He_2

Ronald A. Aziz [a]; Frederick R. W. McCourt [b]; Clement C. K. Wong [b]
[a] Department of Physics, University of Waterloo, Waterloo, Canada [b] Guelph-Waterloo Centre for Graduate Work in Chemistry, University of Waterloo, Waterloo, Canada

Online Publication Date: 20 August 1987

To cite this Article Aziz, Ronald A., McCourt, Frederick R. W. and Wong, Clement C. K.(1987)'A new determination of the ground state interatomic potential for He_2',Molecular Physics,61:6,1487 — 1511
To link to this Article: DOI: 10.1080/00268978700101941
URL: http://dx.doi.org/10.1080/00268978700101941

MOLECULAR PHYSICS, 1987, VOL. 61, NO. 6, 1487–1511

A new determination of the ground state interatomic potential for He_2

by RONALD A. AZIZ
Department of Physics, University of Waterloo,
Waterloo, Ontario, N2L 3G1, Canada

FREDERICK R. W. McCOURT and CLEMENT C. K. WONG
Guelph-Waterloo Centre for Graduate Work in Chemistry,
University of Waterloo, Waterloo, Ontario, N21 3G1, Canada

(*Received 10 February 1987; accepted 31 March 1987*)

A simple accurate potential of the HFD–B form, which appears to be the best characterization of the He–He interaction constructed to date, is presented. It has been fitted to low temperature second virial coefficient data and recent accurate room temperature viscosity data, while at the same time pinning the repulsive wall to the value calculated by Ceperley and Partridge at 1 Bohr. It possesses a well depth of 10·948 K, considerably deeper than many of the recent empirical or *ab initio* potentials. It reproduces, within experimental error, such dilute gas properties as second virial coefficients, viscosities and thermal conductivities over a wide temperature range. It also predicts, within experimental error, such microscopic properties as differential cross sections, high energy integral cross sections and backward glory oscillations in the integral cross sections. Finally, it accounts for nuclear magnetic relaxation in ^{3}He and supports a weakly bound state in the ^{4}He interaction.

1. Introduction

The problem of constructing accurate potential energy functions is an old one which, even for relatively simple interactions such as those between rare gas atoms, has not yet been fully resolved. For the calculation of beam scattering cross sections, second virial coefficients and transport properties of the rare gases to within a few percent, certain model potentials appear to be adequate [1]. Included in this set of model potentials are the Hartree–Fock plus damped dispersion (HFD) [2], the Tang-Toennies (TT) [3] and the exchange coulomb (XC) [4] models. For more accurate calculations, however, it is still necessary to appeal to multiproperty fits [5]. Such an approach was employed for the determination of an accurate He–He potential by Aziz *et al.* [6] in 1979 using the HFD form in conjunction with what were then considered to be the best available experimental data. Their HFDHE2 potential was obtained by fitting accurate second virial coefficients at intermediate temperatures [7] (98 K to 423 K) as well as reliable high-temperature transport coefficient data [8, 9]. It has nearly the correct Hartree–Fock short range repulsion [10] and long-range attraction [11] and supports a single (weakly) bound state [12]. Moreover, it represents well the isotopic differences in the viscosity [13] at temperatures below 100 K (where the transport coefficient data are less reliable) and it predicts differential cross sections reasonably well [14]. Finally, Kalos *et al.* [15], using a Green function Monte Carlo (GFMC) method to calculate the properties of

ground-state ^{4}He, concluded that of the accurate He–He potentials available [6, 14, 16, 17] in 1981, the HFDHE2 potential gave the best agreement with experiment.

Since 1981, additional He–He potentials have been presented. Among them are those of Ng *et al.* [4], Douketis *et al.* [18], Tang and Toennies [19], and Feltgen *et al.* [20]. In particular, the HFIMD potential of [20] was obtained by inversion of the backward glory oscillations appearing in the integral cross sections and associated with the identical particle scattering of ^{4}He and ^{3}He. Feltgen *et al.* employed a physically realistic (but mathematically complicated) two parameter model. In addition to the scattering data (which determined the potential only in the region 1·8 Å to 2·2 Å), the full HFIMD potential also included all available *ab initio* data. It supports a bound state, as does the HFDHE2 potential [12, 20], and coincides with the *ab initio* potentials of Burton [21] and Liu and MacLean [22]. For separations greater than 3 Å, it agrees with the HFDHE2 potential but for separations less than 2 Å, it is considerably softer. An earlier repulsive potential wall obtained by Foreman *et al.* [23], also derived from (high-energy) integral cross-section data, lies between the HFDHE2 and HFIMD potentials, but is closer to the latter than to the former.

There is a growing body of evidence to indicate that the majority of the modern potentials are too repulsive. Firstly, Ceperley and Partridge [24] have employed quantum Monte Carlo methods to determine the exact Born–Oppenheimer interaction energy of two helium atoms with internuclear separations between 0·5 Å and 1·8 Å. Their results indicate that the HFDHE2 potential is too repulsive below 1·8 Å. Secondly, Stebbings and coworkers [25] measured absolute differential cross sections for small-angle elastic scattering in He–He collisions at keV energies and found that their data were consistent with a potential less repulsive than the HFDHE2 potential. Kalos and Whitlock [26] have continued to find nonetheless that, for their GFMC calculations, which depend critically upon the potential well, the HFDHE2 potential remains superior to the HFIMD potential.

In the few years since the HFDHE2 potential was constructed, new virial coefficient data for ^{3}He [27] and ^{4}He [28–31] have been measured at various standards laboratories, new *ab initio* calculations of the dispersion coefficients have appeared [32] in the literature, and new measurements of the transport properties have been made [33–37]. It is now evident that the HFDHE2 potential as well as the newer ones are inadequate [24, 38, 39] to the task of predicting all these data. The thrust for producing a new potential is many-fold, the least of which is the determination of an accurate characterization of the helium interaction. These are:

(1) The International Practical Temperature Scale below 18 K [27–31] is to be redefined in terms of an ideal gas thermometer using helium gas. This requires an accurate knowledge of the virial coefficients, in particular, the second virial coefficient. To this end, many standards laboratories have been measuring them. Rather than expressing the experimental values in terms of an empirical correlation function, it would be preferable [38] to use a potential as the correlating 'instrument'.

(2) The National Bureau of Standards in Washington [40] is redetermining the universal gas constant R from measurements of the sound velocity in helium and argon. To assign an error to their determination, they require a knowledge of the viscosity and thermal conductivity of these gases at the triple point of water (273·16 K). Values derived from an accurate potential would

be more physically based than those expressed in terms of an empirical correlating function.

(3) In many-body studies, the original HFDHE2 potential has served as an excellent 'effective' pair potential, in the sense that pair-wise treatment of the atoms in the condensed phase (neglecting many-body effects) predicts condensed-phase properties reasonably well [15, 26]. Should a newly-determined and more precise potential behave similarly, it might then be possible to draw important conclusions regarding the relative magnitudes of the various short-range and long-range many-body forces [41].

(4) The more recent accurate second virial coefficient data seem to require for their prediction a well depth greater than that of any potential so far obtained by purely *ab initio* methods [21, 22, 42]. This may in fact indicate that a reassessment of *ab initio* methods is in order.

This paper presents a new empirical potential of the HFD–B form which either reproduces or is fully consistent with both short-range and long-range *ab initio* calculations, as well as with second virial coefficient measurements of ^{3}He and ^{4}He over an extended temperature range, and with new more precise transport property measurements. In addition, it accounts well for differential [14, 43] and integral [20, 44, 45] scattering cross section measurements.

2. The HFD–B(HE) potential

The potential form chosen to represent the He–He interaction is the so-called HFD–B form of Aziz and Chen [46] which has certain advantages over the HFD–C form. It is, for example, considered to be a more 'realistic' form in that it reproduces the spectroscopic spacings of the rare gas dimers better than does the HFD–C form [47]. Moreover, it does not 'turn over' and become negative at very small separations.

The form of the HFD–B potential is

$$V(r) = \varepsilon V^*(x), \tag{1}$$

where

$$V^*(x) = A^* \exp(-\alpha^* x + \beta^* x^2) - F(x) \sum_{j=0}^{2} c_{2j+6}/x^{2j+6}, \tag{2}$$

with

$$F(x) = \begin{cases} \exp\left[-\left(\dfrac{D}{x} - 1\right)^2\right], & x < D, \\ 1, & x \geqslant D, \end{cases} \tag{3}$$

where

$$x = \frac{r}{r_m}. \tag{4}$$

For the dispersion coefficients, we have assumed the *ab initio* values of Thakkar and Koide *et al.* [32]. The potential has therefore four adjustable parameters, namely, β,

Table 1.

Parameters for HFD–B(HE) potential	
A^*	1·8443101(5)
α^*	10·43329537
c_6	1·36745214
c_8	0·42123807
c_{10}	0·17473318
C_6/a.u.	1·461
C_8/a.u.	14·11
C_{10}/a.u.	183·5
β^*	−2·27965105
β	−0·259660
D	1·4826
$\frac{\dot{\varepsilon}}{k}\Big/$K	10·948
r_m/A	2·963
σ/A	2·6369

Not all figures displayed are significant. Displayed digits are given specifically for the avoidance of round-off errors. (5) means 10^5.

D, ε, and r_m, determined by fitting the potential to the low temperature (1·47 K to 20·3 K) ^{3}He second virial coefficient data of Matacotta *et al.* [27], the low temperature (2·60 K to 27·1 K) ^{4}He second virial data of Berry [28], and the accurate viscosity data of Vogel [33, 37] (298 K to 641 K), while at the same time pinning the repulsive wall to the value calculated by Ceperley and Partridge [24] at 1·0 Bohr.

We decided to use the accurate viscosity data of Vogel [33, 37] rather than the virial coefficient at 25°C to establish the location of the lower repulsive region of the potential wall because there appears to be no agreement as to what value the virial coefficient should have [7, 48–51]. The viscosity data have stated error bars ranging from 0·1 per cent at 300 K to 0·3 per cent at 600 K. Previous work on neon [52], and on argon and krypton [47] indicate that these error limits are realistic in that potentials consistent with such data are capable of predicting other properties sensitive to the same region of the potential. The parameters of the present potential are given in table 1.

3. Method of calculation

3.1. *Second virial coefficients*

Because of the high degree of accuracy required for the present study, full quantum mechanical virial coefficients have been calculated using established procedures [54–56]. The quantum expressions contain three terms, the perfect gas contribution, the contribution from bound states, and the dynamical contribution associated with the scattering phase shifts. Spin statistics must also be taken into

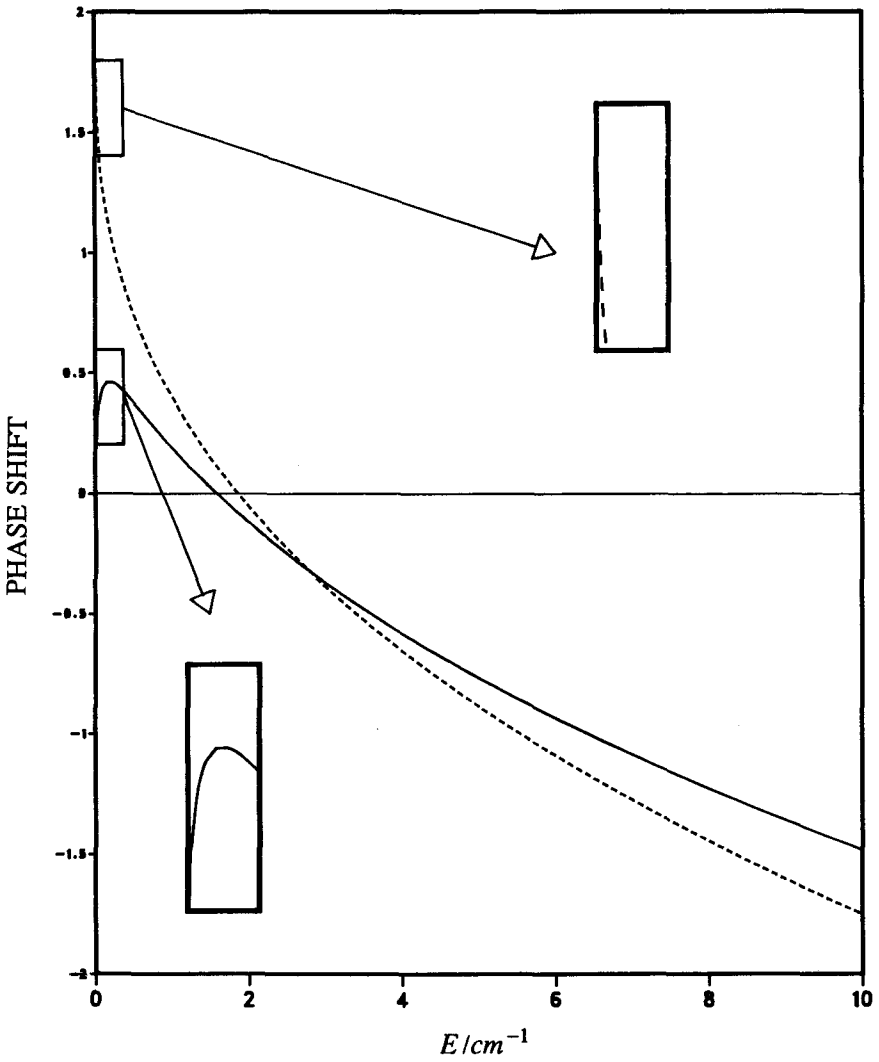

Figure 1. Low energy behaviour of η_0 for ^{4}He–^{4}He scattering (dotted line) and ^{3}He–^{3}He scattering (solid line), showing approach to π and 0, respectively, as $E_k \to 0$.

account so that the second virial coefficient for a boson gas is given by [54]

$$\frac{2I+1}{N}\left(\frac{mk_BT}{\pi\hbar^2}\right)^{3/2} B(T)$$

$$= +\tfrac{1}{2} - 8\sum_n \left\{(I+1)\sum_{l\,\text{even}}(2l+1)\left[\exp\left(-\frac{E^{(-)}_{n,l}}{k_BT}\right)-1\right]\right.$$

$$\left. + I\sum_{l\,\text{odd}}(2l+1)\left[\exp\left(-\frac{E^{(-)}_{n,l}}{k_BT}\right)-1\right]\right\}$$

$$-\frac{8}{\pi}\int_0^\infty \left\{(I+1)\sum_{l\,\text{even}}(2l+1)\eta_l + I\sum_{l\,\text{odd}}(2l+1)\eta_l\right\}\exp(-x)\,dx, \qquad (5a)$$

while that for a fermion gas is given by

$$\frac{2I+1}{N}\left(\frac{mk_B T}{\pi\hbar^2}\right)^{3/2} B(T)$$

$$= -\tfrac{1}{2} - 8\sum_n \left\{ I \sum_{l\,\text{even}} (2l+1)\left[\exp\left(-\frac{E_{n,l}^{(-)}}{k_B T}\right) - 1\right] \right.$$

$$\left. + (I+1)\sum_{l\,\text{odd}} (2l+1)\left[\exp\left(-\frac{E_{n,l}^{(-)}}{k_B T}\right) - 1\right] \right\}$$

$$- \frac{8}{\pi}\int_0^\infty \left\{ I \sum_{l\,\text{even}} (2l+1)\eta_l + (I+1)\sum_{l\,\text{odd}} (2l+1)\eta_l \right\} \exp(-x)\, dx, \qquad (5b)$$

where x is the reduced energy

$$x \equiv \frac{E_k}{k_B T}. \qquad (6)$$

Equation (5*a*), with nuclear spin quantum number $I = 0$, applies to ^{4}He and equation (5*b*), with $I = 1/2$, applies to ^{3}He.

The perfect gas contribution and the bound state contributions are important only at low temperatures. For ^{4}He, our potential supports only a single low-lying bound state at an energy of 1·684 mK, while for ^{3}He, it supports no bound states. The existence or nonexistence of a bound state is reflected in the behaviour of the phase shifts associated with the partial waves for the corresponding orbital angular momentum quantum number via Levinson's theorem [57], which states that the phase shift for a partial wave associated with a bound states changes by π for each bound state in the well. This is clearly illustrated in figure 1 where the phase shift η_0 is plotted as a function of collision energy E_k at low energies. For ^{4}He, the η_0 phase shift approaches π as E_k approaches zero, while for ^{3}He, it goes to zero as E_k approaches zero, in accordance with Levinson's theorem. The approach of η_0 to π for ^{4}He is further illustrated in the inset showing its behaviour near $E_k = 0{\cdot}01\ \text{cm}^{-1}$. The relative importance of the individual contributions to $B(T)$ at low temperatures is illustrated in table 2.

Two independent sets of virial coefficient values are presented. In one of the calculations, the phase shifts were first obtained at a very fine mesh of reduced wave numbers q, specifically, 477 q-values between $q = 0{\cdot}08$ and 27·00 for ^{4}He (between 0·07 and 26·99 for ^{3}He) for the calculation of low-temperature virial coefficients (up to 27 K) and 685 reduced q-values between 0·08 and 80·00 for high-temperature calculations (up to 623 K). Further details of the partitioning of the energy intervals is given in table 3. Thermal averaging was accomplished using a Simpson's rule numerical integration. In the other calculation, the phase shifts were obtained at a slightly coarser energy mesh, using 268 E_k values between 0·01 cm^{-1} (Keysers) and 8000 cm^{-1}, with the thermal averaging carried out using a Simpson's composite rule over energies between 0·01 cm^{-1} and 10·0 cm^{-1} combined with a cubic spline integration over those energies above 10·0 cm^{-1}. Further details regarding these meshes may also be found in table 3. The two sets almost converge. For example, for ^{3}He at 1·47 K, the two sets of calculations differ by only 0·26 cc/mol in 174 cc/mol, and are practically identical at 20 K. Differences at room temperature are in the order of 0·04 cc/mol in 12 cc/mol.

Table 2. Various contributions to the second virial coefficient of helium-4 on the basis of the HFD–B(HE) potential

T (K)	B (ideal)	B (binding)	B (phase shift)	B (total)
3·00	−13·61	−0·122	−106·22	−119·95
4·00	−8·84	−0·060	−76·08	−84·98
5·00	−6·33	−0·034	−57·93	−64·29
8·00	−3·13	−0·011	−30·30	−33·43
10·00	−2·24	−0·006	−20·93	−23·17
15·00	−1·22	−0·002	−8·33	−9·55
20·00	−0·79	−0·001	−2·01	−2·80
27·00	−0·50	−0·001	2·85	2·35
30·00	−0·43	−0·000	4·22	3·79
35·00	−0·34	−0·000	5·94	5·60
40·00	−0·28	−0·000	7·21	6·93
50·00	−0·20	−0·000	8·91	8·71
60·00	−0·15	−0·000	9·98	9·82
70·00	−0·12	−0·000	10·68	10·56
80·00	−0·10	−0·000	11·16	11·06
90·00	−0·08	−0·000	11·49	11·41
100·00	−0·07	−0·000	11·74	11·67
125·00	−0·05	−0·000	12·07	12·02
150·00	−0·04	−0·000	12·20	12·16
175·00	−0·03	−0·000	12·23	12·20
200·00	−0·03	−0·000	12·20	12·17
250·00	−0·02	−0·000	12·04	12·02
300·00	−0·01	−0·000	11·85	11·84

Table 3.

From	To	Step size	From	To	Step size
		q-Integration mesh for virial calculations			
0·08	3·00	0·020	27·00	61·0	0·200
3·00	6·00	0·025	61·0	80·0	0·050
6·00	27·00	0·100			
		E_k-Integration mesh for virial calculations			
0·01	0·10	0·0025	30·0	100·0	5·0
0·10	1·00	0·050	100·0	200·0	10·0
1·00	6·00	0·10	200·0	1000·0	20·0
6·00	20·0	0·50	1000·0	2000·0	50·0
20·0	30·0	1·0	2000·0	8000·0	100·0
		E_k-Integration mesh for T_1 calculation in ^{3}He			
0·01	0·10	0·0025	20·0	30·0	1·0
0·10	1·0	0·050	30·0	100·0	5·0
1·0	6·0	0·100	100·0	200.0	10·0
6·0	20·0	0·500	200·0	1000·0	20·0

3.2. *Transport properties*

Quantum temperature-dependent reduced cross sections have been calculated using an adaptation of the classical reduced integral program of O'Hara and Smith [59]. In this approach, a Chebyshev approximation is found for the quantal cross sections which are calculated using standard formulas [60] which include appropri-

ate spin and statistical effects [61]. The required phase shifts were obtained using the quantal phase shift routine of LeRoy [62] which employs a numerical integration and a Gaussian quadrature of the JWKB correction to the phase shift. The Clenshaw–Curtis quadrature [58] was used to perform the energy integration in the required collision integrals [61]. O'Hara and Smith argue that this approach is very efficient and reliable because Clenshaw–Curtis integration is almost as accurate as gaussian quadratures for the same number of abscissae and, in addition, the abscissae for higher order integrations overlap those of lower order integrations. An important feature of the Clenshaw–Curtis quadrature is its error estimate. This reliable estimate is based on the same function evaluations needed in the quadrature formula. Therefore, only the computation necessary to achieve a specified accuracy is done. Third Chapman–Cowling approximation expressions [63] have been used to calculate the viscosity and thermal conductivity coefficients for comparison with experimental values.

3.3. *Nuclear magnetic relaxation*

The ^{3}He nucleus possesses a nuclear spin $I = \frac{1}{2}$ whereas the ^{4}He nucleus has nuclear spin $I = 0$, and consequently ^{3}He gas has a nuclear magnetization. As a consequence of the nonzero nuclear spin, two colliding ^{3}He atoms may form either a singlet or a triplet nuclear spin state. In the singlet state, with $I_T = 0$, the interaction is simply $V(r)$ but, in the triplet state, with $I_T = 1$, the atoms also interact weakly via the magnetic dipole–dipole interaction and, in principle, also via a spin–rotation interaction (rotation of the short-lived $^3He_2$ collision pair) so that the interaction potential is

$$V(\mathbf{r}, \mathbf{I}) = V(r) + V_{mag}(\mathbf{r}, \mathbf{I}_T), \tag{7}$$

where V_{mag} is orders of magnitude smaller than the central potential $V(r)$ which we have been discussing earlier.

Traditional nuclear spin relaxation experiments were first carried out on ^{3}He gas by Chapman and Richards [64]. They determined that the relaxation mechanism was that of dipolar relaxation [65]. As expected, the longitudinal relaxation time T_1 was found to be very long. A kinetic theory description of the dipolar relaxation in ^{3}He was given in 1967 by Chen and Snider [66] and a detailed numerical calculation of T_1, using the McLaughlin–Schaefer (MS) [10] and Beck [16] potentials was first made by Shizgal [67]. He used a distorted-wave Born treatment with the dipole–dipole interaction serving as the perturbation.

Recent measurements of T_1 in ^{3}He at low temperatures were made by Chapman [68]. He also used Shizgal's code and compared his data with values of T_1 calculated from the MS [10], Beck [16] and Bruch–McGee [17] potentials. He obtained good agreement between measured and calculated values of T_1. We have performed essentially the same calculations as Shizgal and Chapman for the Beck and MS potentials as well as for the HFDHE2 potential of Aziz *et al.* [6] and the present HFD–B potential.

Our distorted-wave Born approximation (DWBA) calculations were based upon formulae given by Shizgal [67], properly allowing for the fact that relaxation only occurs via those collisions which correspond to the formation of a triplet nuclear spin state of the $^3He_2$ complex (in which the dipolar relaxation mechanism is operative). In calculating the accurate wave functions required at each collision energy, we have used a modification of the Le Roy phase shift-time delay code [62], starting our integration from the inner turning point and employing 8000 steps in the outward integration. The actual step size depends upon the energy at which the

Table 4.

R (au)	from scattering [23]	*Ab initio* [24]	HFD–B(HE)	HFDHE2 [6]
	Strongly repulsive region of helium potential (in K)			
1·00	308 500	291 900	291 300	543 800
1·25	182 900	174 600	175 500	299 900
1·50	108 500	105 000	104 800	165 300
1·75	64 330	61 400	61 990	91 120
2·00	38 150	35 800	36 340	50 090
2·25	22 620	20 950	21 090	27 360
2·50	13 410	11 920	12 100	14 820
2·75	7955		6852	7962
2·8346	6666	5540	5633	6439
3·00	4717	3800	3819	4240

calculation is made. We have employed 228 collision energies spanning the range 0·01 cm^{-1} to 1000 cm^{-1} for the energy averages. As in one set of virial coefficient calculations, we have combined a composite Simpson's rule integration from 0·01 cm^{-1} to 10·0 cm^{-1} and a cubic spline integration from 10·0 cm^{-1} to 1000 cm^{-1}. Further details on the mesh can be found in table 3.

4. Results and discussion

4.1. *Repulsive wall*

The repulsive wall of our potential was pinned at an internuclear separation of one Bohr to the value obtained by Ceperley and Partridge using quantum Monte Carlo techniques to determine the Born–Oppenheimer interaction energies at separations of 1·0 to 3·0 Bohr. In table 4, we present a comparison between values for the repulsive wall of the new HFD–B(HE) and the earlier HFDHE2 potentials with the interaction energies calculated by Ceperley and Partridge [24] at the same separations. Also shown are the results inferred from high energy integral cross-section measurements of Foreman *et al.* [23]. As might be expected from our fitting procedure, our values are in excellent agreement with those of reference [24] for the whole range of separations. Our potential lies somewhat lower than the scattering potential especially at larger separations but is certainly in better agreement with it than is the earlier potential of Aziz *et al.* [6]. The repulsive walls of the HFD–B(HE) and HFDHE2 potentials are shown in figure 2 along with that obtained by Foreman *et al.* [23] from high energy integral cross section measurements.

4.2. *Second virial coefficients*

Probably the most reliable low temperature virial coefficients for ^4He are those of Berry [28] which, in the range 2·6 to 27·1 K, have error bars ranging from 1 to 0·2 cc/mol. Smoothed fits to these data have been provided by Plumb [30] and by Steur [69] (the latter is a surface fit to the data of Berry [28], Kemp *et al.* [70] and Kell *et al.* [49]). Other data considered include those of Kemp *et al.* [70] (27·1 to 172 K); those of Kell *et al.* [49] (values at 298·15 and 623·15 K), Holste *et al.* 1980 [50] (100 to 300 K) and NBS values (273 to 423 K) as cited by Guildner and Edsinger [51].

Recent data for ^3He have been obtained by Matacotta *et al.* [27] for the range 1·47 to 20·3 K with error bars ranging from ±0·5 cc/mol at 1·5 K to ±0·2 cc/mol at

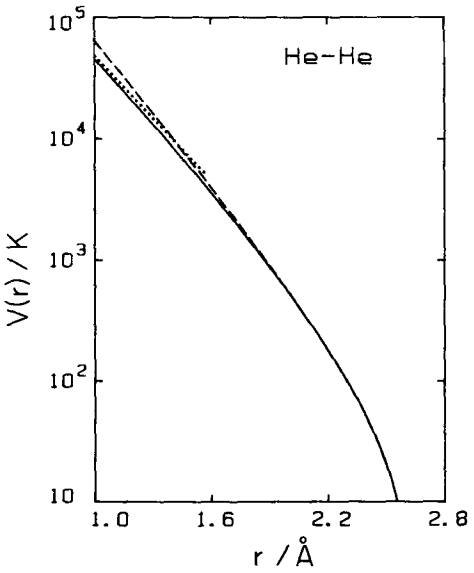

Figure 2. Behaviour of the repulsive walls for the HFD–B(HE) (solid line), HFDHE2 (dashed line) potentials together with the repulsive wall obtained in [23] from inversion of high-energy integral cross section data (dotted line).

20·3 K. Revised values corrected for the third virial coefficient have been determined by McConville [71] and smoothed by us by a least squares procedure. The high temperature data have been determined by the Burnett method. In addition, Gammon [7] presented values from 98 to 423 K derived from acoustic measurements.

In table 5, we present various sets of data, their corresponding error bars and the deviations of the predictions based on the present potential. It predicts, in addition to the data of Berry [28] and Matacotta *et al.* [27] to which it was fitted, the data of Kell *et al.* [49], Kemp *et al.* [70], Gammon [7] and Holste *et al.* [50] to within experimental error. The predicted sets of data encompass the extensive temperature range from 1·47 to 623 K! The value of the second virial coefficient of Waxman and Davis [48] at 298·15 K appears to be too high by about 0·05 cc/mol, or about four times their estimated error. The values determined at this temperature by Kell *et al.* (11·83 $\pm$ 0·03 cc/mol), Gammon (11·86 $\pm$ 0·05 cc/mol) and Holste *et al.* (11·81 $\pm$ 0·1 cc/mol) are all lower; the predictions based on our potential agree with all of these measurements, given their less optimistic error bounds. Agreement with the recent measurements of Cameron and Seidel [72] is less satisfactory. Deviation plots for ^{4}He and ^{3}He are given in figures 3 and 4, respectively. The HFDHE2 potential clearly does not fare as well as does the new HFD–B(HE) potential, especially at low temperatures.

4.3. *Transport data*

4.3.1. *Viscosity*

In addition to reproducing the single value of the viscosity at 300 K which was used in its determination, the present HFD–B(HE) potential also predicts to within

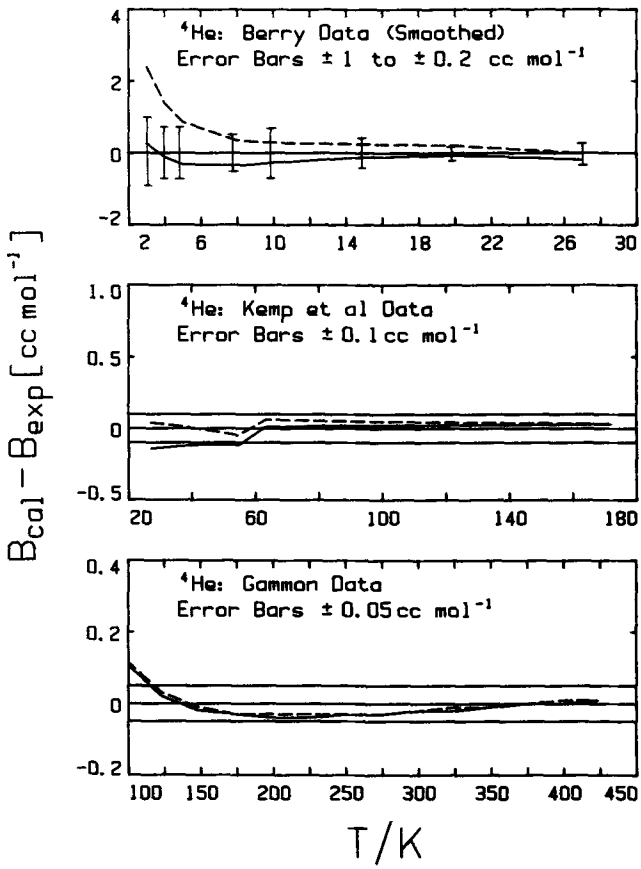

Figure 3. Deviation plots for ^{4}He second virial coefficient. Deviations from the data of Berry [28] (upper plot), Kemp *et al.* [70] (middle plot) and Gammon [7] (lower plot). Potentials identified as in figure 2.

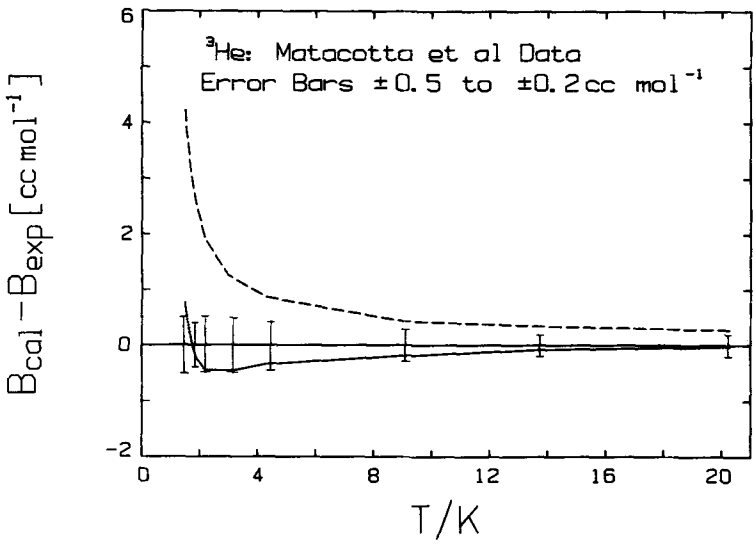

Figure 4. Deviation plots for ^{3}He second virial coefficient. Deviations from the data of Matacotta *et al.* [27]. Potentials identified as in figure 2.

Table 5. Predictions of second virial coefficients by HFD–B potential.

	T (K)	B (exp)	ΔB	B (calc1)	B (calc1)–B (exp)	B (calc2)	B (calc2)–B (exp)
				Helium-4			
Berry [28]	2·60	−142·5	1·0	−141·94	0·56	−142·36	0·14
(raw data)	2·75	−133·2	0·7	−132·89	0·31	−133·26	−0·06
	3·33	−105·8	0·7	−105·99	−0·19	−106·23	−0·43
	4·22	−79·5	0·5	−79·57	−0·07	−79·84	−0·34
	7·20	−39·0	0·7	−39·14	−0·14	−39·15	−0·15
	13·80	−11·7	0·4	−11·91	−0·21	−11·91	−0·21
	20·27	−2·4	0·2	−2·54	−0·14	−2·53	−0·13
	27·10	2·5	0·3	2·40	−0·10	2·40	−0·10
Berry [28, 69]	2·60	−142·44	1·0	−141·94	0·50	−142·36	0·08
(Surface fit)	2·75	−133·33	0·7	−132·89	0·44	−133·26	0·07
	3·33	−106·35	0·7	−105·99	0·36	−106·23	0·12
	4·22	−79·82	0·5	−79·57	0·25	−79·84	−0·02
	7·20	−39·15	0·7	−39·14	0·01	−39·15	0·01
	13·80	−11·83	0·4	−11·91	−0·08	−11·91	−0·08
	20·27	−2·48	0·2	−2·54	−0·06	−2·53	−0·05
	27·10	2·42	0·3	2·40	−0·02	2·40	−0·02
Berry [28, 30]	3·00	−120·21	1·0	−119·95	0·26	−120·04	0·17
(Smoothed)	4·00	−84·86	0·7	−84·98	−0·12	−85·05	−0·18
	5·00	−63·97	0·7	−64·29	−0·32	−64·33	−0·36
	8·00	−33·08	0·5	−33·43	−0·35	−33·45	−0·32
	10·00	−22·91	0·7	−23·17	−0·26	−23·18	−0·27
	15·00	−9·44	0·4	−9·55	−0·11	−9·54	−0·10
	20·00	−2·74	0·2	−2·80	−0·06	−2·80	−0·06
	27·00	2·54	0·3	2·35	−0·19	2·35	−0·19
Gugan [29, 30]	3·00	−120·52	1·0	−119·95	0·57	−120·04	0·48
(Smoothed)	4·00	−85·20	0·7	−84·98	0·22	−85·05	0·15
	5·00	−64·32	0·7	−64·29	0·03	−64·33	0·01
	8·00	−33·28	0·5	−33·43	−0·15	−33·45	−0·17

	10·00	−23·02	0·7	−23·17	−0·15	−23·18	−0·16
	15·00	−9·44	0·4	−9·55	−0·11	−9·54	−0·10
	20·00	−2·72	0·2	−2·80	−0·08	−2·80	−0·08
	27·00	2·41	0·3	2·35	−0·06	2·35	0·06
Kemp *et al.* [70]	27·097	2·47	0·06	2·40	−0·07	2·40	−0·07
	43·794	7·80	0·11	7·71	−0·09	7·71	−0·09
	54·358	9·28	0·07	9·24	−0·04	9·25	−0·03
	63·150	10·01	0·09	10·07	0·06	10·07	0·06
	82·804	11·13	0·11	11·18	0·05	11·19	0·06
	172·011	12·15	0·14	12·17	0·02	12·17	0·02
Gammon [7]	98·15	11·522	0·05	11·628	0·11	11·598	0·08
	123·15	11·984	0·05	12·007	0·02	11·977	−0·01
	148·15	12·174	0·05	12·159	−0·02	12·131	−0·04
	173·15	12·228	0·05	12·195	−0·03	12·170	−0·06
	198·15	12·209	0·05	12·172	−0·04	12·147	−0·06
	223·15	12·148	0·05	12·112	−0·04	12·088	−0·06
	248·15	12·065	0·05	12·032	−0·03	12·009	−0·06
	273·15	11·968	0·05	11·940	−0·03	11·917	−0·05
	298·15	11·863	0.05	11·842	−0·02	11·820	−0·04
	323·15	11·756	0·05	11·740	−0·02	11·719	−0·04
	348·15	11·647	0·05	11·639	−0·01	11·617	−0·03
	373·15	11·539	0·05	11·536	0·00	11·514	−0·02
	398·15	11·433	0·05	11·434	0·00	11·413	−0·02
	423·15	11·329	0·05	11·335	0·01	11·313	−0·02
Kell *et al.* [49]	298·15	11·83	0·03	11·84	0·01	11·82	−0·01
	623·15	10·61	0·01	10·61	0·00	10·60	−0·01
Holste *et al.* [50]	100·00	11·30	0·3	11·67	0·37	11·64	0·34
	125·00	11·90	0·3	12·02	0·12	11·99	0·09
	150·00	12·10	0·3	12·16	0·06	12·14	0·04
	175·00	12·12	0·3	12·20	0·08	12·17	0·05
	200·00	12·10	0·3	12·17	0·07	12·14	0·04
	225·00	12·06	0·3	12·11	0·05	12·08	0·02
	250·00	12·02	0·3	12·02	0·00	12·00	−0·02
	273·15	11·95	0·3	11·94	−0·01	11·92	−0·03
	275·00	11·94	0·3	11·93	−0·01	11·91	−0·03
	300·00	11·81	0·3	11·84	0·03	11·81	0·00

Table 5 (*continued*).

	T (K)	B (exp)	ΔB	B (calc1)	B (calc1)–B (exp)	B (calc2)	B (calc2)–B (exp)
				Helium-4			
Waxman and Davis [48]	298·15	11·89	0·012	11·84	−0·05	11·82	−0·07
Guildner and Edsinger [51]	273·15	12·00		11·94	−0·06	11·92	−0·08
	298·15	11·89		11·84	−0·05	11·82	−0·07
	323·15	11·77		11·74	−0·03	11·72	−0·05
	348·15	11·67		11·64	−0·03	11·62	−0·05
	373·15	11·56		11·54	−0·02	11·52	−0·04
	398·15	11·46		11·43	−0·03	11·42	−0·04
	423·15	11·36		11·34	−0·03	11·32	−0·04
				Helium-3			
Matacotta *et al.* [27]	1·500	−171·60	0·5	−170·84	0·76	−171·08	0·52
	1·550	−166·53	0·5	−165·98	0·55	−166·20	0·33
	1·730	−150·35	0·4	−150·32	0·03	−150·48	−0·13
	1·900	−137·46	0·4	−137·71	−0·24	−137·84	−0·38
	2·200	−118·97	0·5	−119·42	−0·45	−119·51	−0·54
	3·000	−86·03	0·5	−86·50	−0·46	−86·54	−0·51
	4·300	−56·93	0·4	−57·26	−0·33	−57·28	−0·35
	9·000	−19·65	0·3	−19·83	−0·18	−19·83	−0·18
	13·800	−7·26	0·2	−7·33	−0·07	−7·33	−0·07
	20·300	0·31	0·2	0·29	−0·02	0·29	−0·02
Matacotta *et al.* [27, 71]†	1·470	−173·58	0·5	−173·87	−0·29	−174·12	−0·54
	1·500	−170·54	0·5	−170·84	−0·30	−171·08	−0·54
	1·550	−165·68	0·5	−165·98	−0·30	−166·20	−0·52
	1·730	−149·99	0·4	−150·32	−0·33	−150·48	−0·49
	1·900	−137·37	0·4	−137·71	−0·34	−137·84	−0·47
	2·200	−119·12	0·5	−119·42	−0·30	−119·51	−0·39

	3·000	−86·31	0·5	−86·50	−0·19	−86·54	−0·23
	4·300	−57·15	0·4	−57·26	−0·11	−57·28	−0·13
	9·000	−19·75	0·3	−19·83	−0·08	−19·83	−0·13
	13·800	−7·33	0·2	−7·33	0·00	−7·33	0·00
	20·300	0·24	0·2	0·29	0·05	0·29	0·05
Matacotta *et al.* [27, 71]‡	1·470	−173·62	0·5	−173·87	−0·25	−174·12	−0·50
	1·500	−170·55	0·5	−170·84	−0·29	−171·08	−0·53
	1·550	−165·64	0·5	−165·98	−0·34	−166·20	−0·56
	1·730	−149·86	0·4	−150·32	−0·46	−150·48	−0·62
	1·900	−137·22	0·4	−137·71	−0·49	−137·84	−0·62
	2·200	−118·97	0·5	−119·42	−0·45	−119·51	−0·54
	3·000	−86·25	0·5	−86·50	−0·25	−86·54	−0·29
	4·300	−57·16	0·4	−57·26	−0·10	−57·28	−0·12
	9·000	−19·78	0·3	−19·83	−0·05	−19·83	−0·05
	13·800	−7·34	0·2	−7·33	0·01	−7·33	0·01
	20·300	0·25	0·2	0·29	0·04	0·29	0·04
Cameron and Seidel [72]	0·631	−650·0	170	−319·6	330·0	−321·7	328·3
	0·806	−274·0	14	−275·1	−1·1	−276·2	−2·24
	1·038	−222·4	6·9	−230·3	−7·9	−230·9	−8·5
	1·214	−194·7	2·8	−204·0	−9·2	−204·4	−9·7
	1·307	−182·5	3·3	−192·1	−9·6	−192·4	−9·9

† Data of [27] corrected for third virial coefficient [71] and smoothed by least squares.
‡ Selected data of [27] corrected for third virial coefficient [71] and smoothed by least squares.

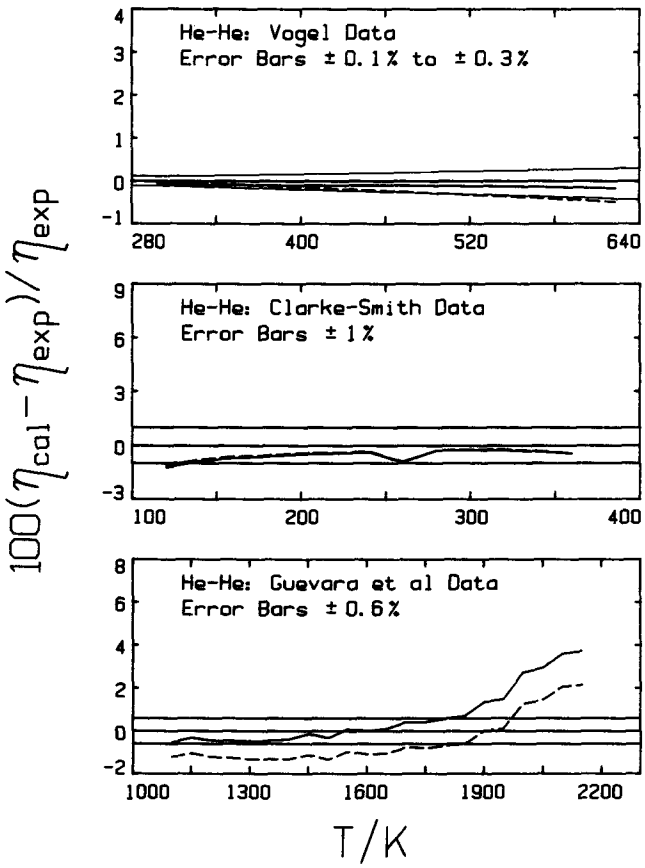

Figure 5. Deviation plots for viscosity: Percentage deviation from data of Vogel [33] (upper plot), Clarke and Smith [73] (middle plot) and Guevara *et al.* [74] (lower plot).

±0·2 per cent the other highly accurate viscosity measurements of Vogel [33, 37], as well as the intermediate temperature (77 K–300 K) viscosity data of Clarke and Smith [73] (77 to 300 K) to within ±1 per cent and the high temperature (1100 K–1800 K) viscosity data of Guevara *et al.* [74] to within ±0·6 per cent. Above 1800 K, where temperature assignment is probably difficult, the deviations between calculated and experimental results would appear to suggest a potential which is too repulsive, even though the present potential is consistent with the interaction energies calculated by Ceperley and Partridge for the full range of separations (1·0–3·0 Bohr) of their calculations. In this context, it is perhaps interesting to note that the Los Alamos viscosity measurements for neon, argon, and krypton also demonstrate the same behaviour above 1800 K [75, 74, 76] with respect to other recent potentials. It does not agree particularly well with the older low temperature viscosity data but, as these data are considered to be unreliable (cf. [6]), we have ignored them. Deviation plots for both the HFDHE2 and HFD–B(HE) potentials are given in figure 5. As can be seen, calculations based upon the current HFD–B(HE) potential give better agreement with the experimental data at all temperatures below 1800 K than do calculations based upon the HFDHE2 potential.

Table 6. Rms deviations for selected transport properties of helium-4

Data	Temperature range (K)	Error bars (per cent)	Rms deviation	Maximum ±per cent deviation
		Viscosity	/μP	
Vogel [33]	298–623	±0·1 to ±0·3	0·340(0·12)	−0·04 to −0·17
Vogel [37]†	298–641	±0·1 to ±0·3	0·146(0·05)	−0·02 to −0·11
Clarke and Smith [73]	77–374	±1	0·825(0·57)	−0·20 to −1·0
Clarke and Smith [73] (smoothed)	120–360	±1	0·934(0·63)	−0·25 to −1·2
Guevara *et al.* [74]	1100–1800	±0·6	2·32(0·38)	−0·53 to 0·59
Guevara *et al.* [74]	1100–2150	±0·6	11·4(1·50)	−0·53 to 3·7
Kestin *et al.* [36]	300·65	±0·3	0·218(0·11)	−0·11
		Thermal conductivity/mW $(mK)^{-1}$		
Assael *et al.* [35]	308·15	±0·2	0·21(0·13)	0·13
Kestin *et al.* [36]	300·65	±0·3	0·11(0·07)	0·07
Acton and Kellner [34]	4–20	±1·1	0·11(0·73)	−1·2 to 0·34
Acton and Kellner [34] (smoothed)	4–20	±1·1	0·10(0·68)	−1·0 to 0·37
Haarman [77]	328–468	±0·3	0·64(0·33)	0·21 to 0·42
Jody *et al.* [8]	400–2500	±2·0 to ±4·7	10·8(2·25)	−0·05 to 4·8

† Data obtained using edge-correction C.
Values in parentheses refer to rms percentage deviation.

4.3.2. *Thermal conductivity*

Although earlier viscosity data below 77 K may not be reliable, recent low temperature thermal conductivity data, which depend upon the same $\Omega^{(2,2)*}$ collision integral as does the viscosity [63], obtained by Acton and Kellner [34] have stated accuracies of ±1·1 per cent. There is, however, appreciable scatter in their measurements and as a result, we have smoothed the data using a least squares procedure. The thermal conductivities are predicted by our potential to within experimental error (the raw data to ±1·1 per cent and the smoothed data to ±1·0 per cent). Other thermal conductivity data considered are those of Assael *et al.* [35], Kestin *et al.* [36], Haarman [77], and Jody *et al.* [8]. The data of Haarman, obtained using a transient hot-wire technique, are not quite predicted to within experimental error but the more recent data of Kestin *et al.* [36] and Assael *et al.* [35], who used the same technique but with an improved apparatus, are predicted to within their stated error bounds (±0·3 and ±0·2 per cent respectively). Details of the rms and rms percentage deviations for the transport properties are given in table 6.

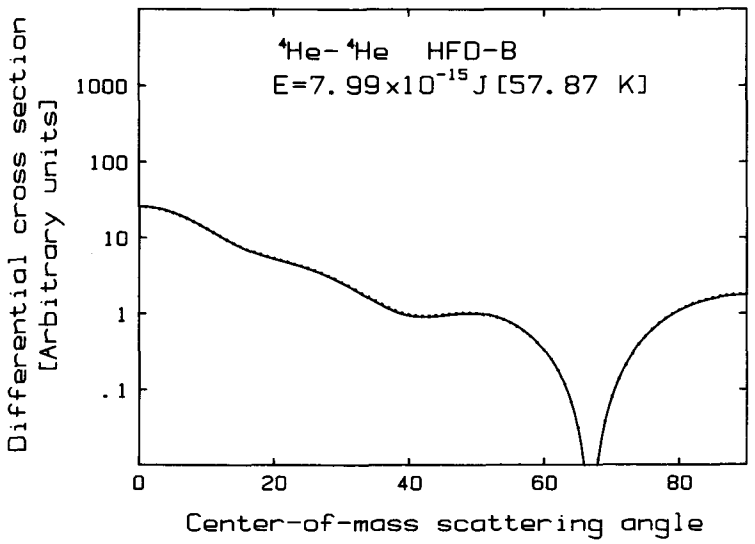

Figure 6. Differential cross section for ^{4}He–^{4}He scattering at $E_k = 57{\cdot}87$ K as calculated from the HFD–B(HE) potential (solid line) and from the ESMSV fitted potential (points) given in [14, 43].

4.3. *Differential cross sections*

Differential collision cross sections were measured for crossed beams of ^{4}He–^{4}He by Farrar and Lee [43] and for ^{3}He–^{4}He by Burgmans *et al.* [14]. To assess the ability of a potential to predict differential collision cross section (DCCS) data, the best approach would be to predict values in the laboratory frame-of-reference, averaging over the appropriate experimental conditions. Since sufficient information to allow such a calculation to be performed was not available to us, we have taken a different approach [78]. The ESMSV(^{4}He–^{4}He) [43, 14] and ESMMSV(^{3}He–^{4}He) [14] potentials which were fitted to the original data have been employed to generate pseudodata in the centre-of-mass frame of reference. The pseudodata generated in this way have then been treated as standard data with which predictions based on other potentials may be compared. The use of such pseudodata for testing the present potential construct depends upon the accuracy with which the experimental fit potential describes the beam data. Any averaging over the experimental conditions would be expected to mask the differences between the two calculated values to some extent. The results for the HFD–B potential are presented in figures 6–8 with the dotted line representing the pseudodata. The agreement is seen to be excellent, especially for low relative energies for both the ^{4}He–^{4}He and ^{3}He–^{4}He cases.

4.4. *Integral collision cross sections*

Integral collision cross sections were measured for crossed beams of ^{4}He–^{4}He and ^{3}He–^{3}He by both the Bonn [44] and Goettingen [20] groups as well as for ^{3}He–^{4}He crossed beams by the latter group. This property is treated in a way analogous to that used for calculating the DCCS. The results are presented in figures 9, 10. In the case of the ^{4}He–^{4}He scattering we show the pseudodata

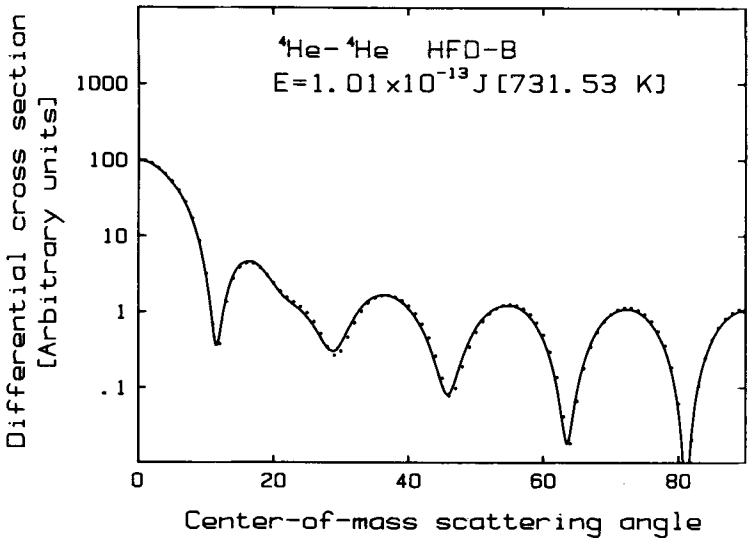

Figure 7. Differential cross section for ^{4}He–^{4}He scattering at $E_k = 731{\cdot}53$ K as calculated from the HFD–B(HE) potential (solid line) and from the ESMSV fitted potential (points) given in [43].

obtained using the potential obtained from inversion of the pure ^{4}He scattering data (solid circles), together with the results obtained using the HFD–B(HE) potential reported here and the results obtained using the recommended HFIMD potential from [20]. For the ^{3}He–^{3}He scattering, we show only the results of calculations with the present HFD–B(HE) potential and the HFIMD potential of [20]. In the first case, we see that the solid curve representing the HFD–B(HE) potential and the

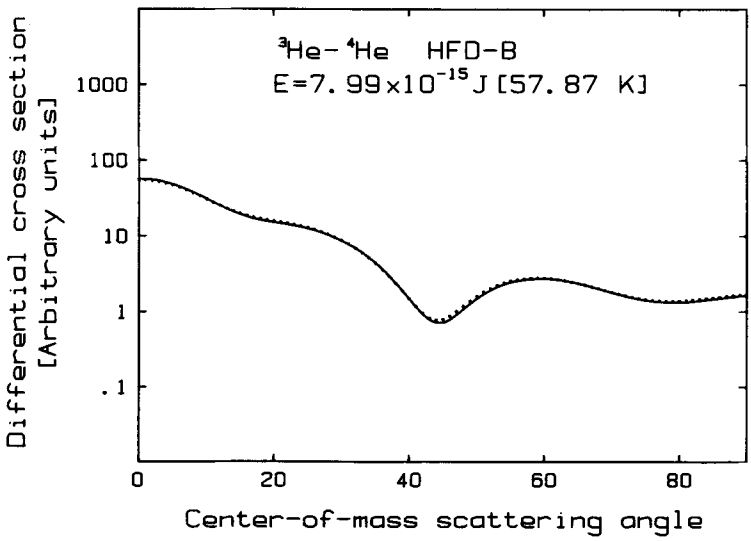

Figure 8. Differential cross section for ^{4}He–^{3}He scattering at $E_k = 57{\cdot}87$ K as calculated from the HFD–B(HE) potential (solid line) and from the ESMMSV potential (points) of [14].

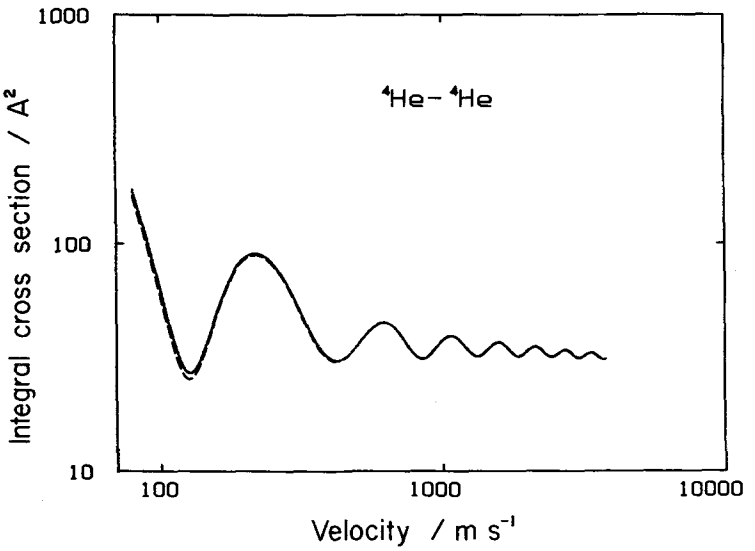

Figure 9. Integral cross section as a function of relative speed for ^{4}He–^{4}He as calculated from the HFD–B(HE) potential (solid line), the HFIMD potential (dashed line). Included also are pseudodata (dots) calculated from the reference potential obtained by Feltgen *et al.* [20] from inversion of their ^{4}He–^{4}He scattering data: However, they cannot easily be distinguished on the scale of this figure as they are masked by the solid line.

pseudodata overlap, while the HFIMD results lie considerably lower at low velocities. In the second case, we see that the results of the HFD–B(HE) calculations lie above the HFIMD results. For both ^{4}He–^{4}He and ^{3}He–^{3}He scattering, the HFD–

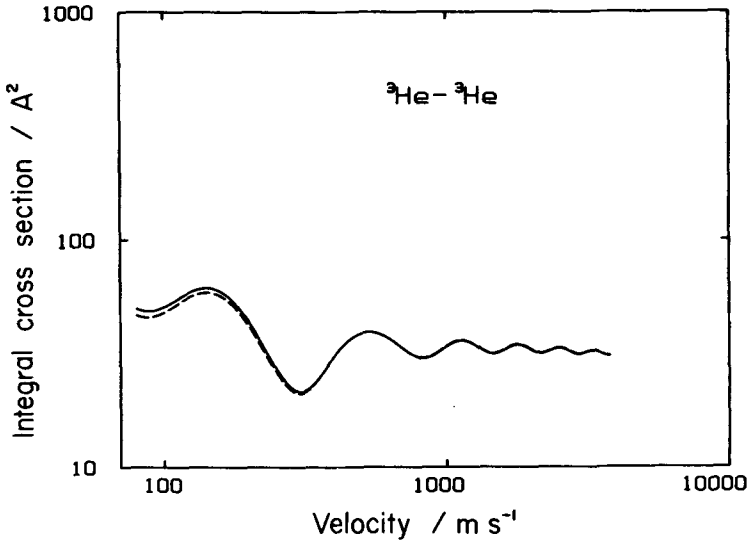

Figure 10. Integral cross section as a function of relative speed for ^{3}He–^{3}He scattering as calculated from the HFD–B(HE) potential (solid line) and the HFIMD potential (dashed line). No pseudodata are shown in this case, since we were unable to obtain an appropriate reference potential from [20].

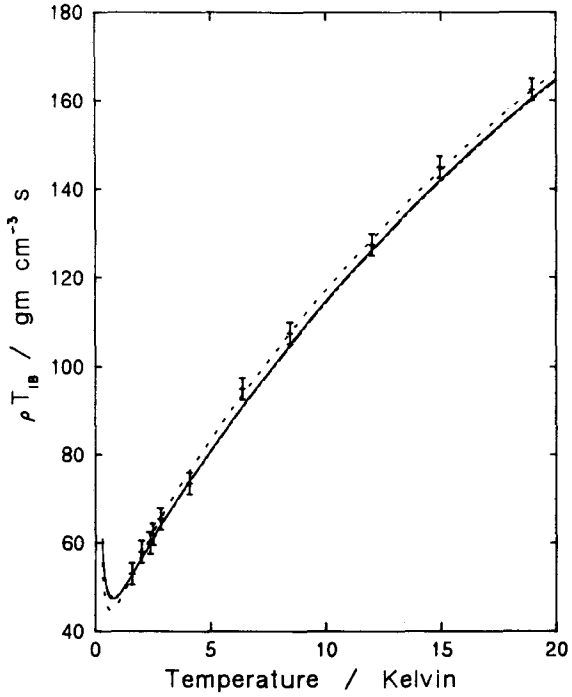

Figure 11. Behavour of the longitudinal relaxation time T_1 as a function of temperature as calculated using the MS, HFDHE2 and HFD–B(HE) potentials. The calculations for the HFDHE2 and HFD–B(HE) potentials are almost superimposed. Also shown in this figure are the experimental data of Chapman [68]. ——, HFD–B(HE); — —, HFDHE2; – – –, MS.

B(HE) calculations are closer to the experimental results than are the HFIMD calculations. It is possible that this difference is merely due to an incorrect c_6 value used in the HFIMD potential.

4.5. *Nuclear magnetic relaxation in ^3He*

The results of our calculations of ρT_1 (ρ is the helium gas density in gm cm^{-3}) for the MS, HFDHE2 and HFD–B(HE) potentials are displayed in figure 11. Unfortunately, Chapman's [68] raw data were never published, so that we have had to extract experimental values of ρT_1 from his figure 6. Moreover, we have assigned (optimistically) error bars of $\pm 2{\cdot}5\,\mathrm{gm\,cm^{-3}\,s}$ to the values so extracted. All three potentials give results which are in fairly good agreement with the experimental values, the results for the MS potential faring somewhat better than the (indistinguishable) results obtained from the HFDHE2 and HFD–B(HE) potentials. Because of this, the N.M.R. data do not provide us with as strong a check on the potential as we would like. Shizgal [79] has also pointed out that the value $T_{1,\min}$ which occurs at $T_{\min}$ is quite sensitive to the values of the potential parameters σ and ε. In view of the fact that all other properties for He are relatively insensitive to the precise value of ε, accurate measurements of T_1 in the vicinity of the minimum would provide useful bounds on the correct value of ε. Finally, since both the spherical He–He interaction is now so accurately known and experimental values of

Table 7. Calculated integral cross sections (/A^2) for selected potentials.

Primary beam velocity /m sec^{-1}	^{4}He–^{4}He				^{3}He–^{3}He		
	Feltgen–4† Pseudodata	HFD–B (Calculated–pseudodata)	HFDHE2 (Calculated–pseudodata)	HFIMD (Calculated–pseudodata)	HFD–B Calculated	HFDHE2 Differences‡	HFIMD Differences‡
80	172·56	−1·47	−7·71	−11·13	50·07	−2·18	−3·21
85	134·69	−1·22	−6·37	−9·22	48·93	−2·04	−2·97
90	104·98	−1·01	−5·26	−7·64	48·85	−1·96	−2·83
95	81·79	−0·83	−4·34	−6·31	49·57	−1·91	−2·74
100	63·91	−0·68	−3·57	−5·21	50·88	−1·90	−2·70
120	29·46	−0·30	−1·66	−2·37	57·98	−1·98	−2·76
140	31·65	−0·14	−1·03	−1·26	61·64	−1·98	−2·76
160	51·23	−0·13	−1·13	−1·16	59·04	−1·81	−2·54
180	73·20	−0·20	−1·49	−1·49	52·08	−1·53	−2·17
200	87·38	−0·25	−1·67	−1·74	43·67	−1·23	−1·77
240	86·90	−0·25	−1·47	−1·72	29·63	−0·76	−1·09
280	67·59	−0·20	−1·09	−1·45	22·56	−0·44	−0·60
320	48·29	−0·15	−0·79	−1·16	21·83	−0·26	−0·26
360	36·21	−0·11	−0·62	−0·87	25·40	−0·17	−0·06
400	31·26	−0·08	−0·50	−0·57	30·61	−0·16	+0·03
440	31·04	−0·06	−0·37	−0·26	35·21	−0·15	+0·07
480	33·77	−0·03	−0·24	+0·01	38·18	−0·14	+0·06
520	38·03	−0·01	−0·16	+0·17	39·43	−0·13	+0·03

† Potential fitted to ^{4}He–^{4}He data by Feltgen *et al.* [20].
‡ Only the differences between the present HFD–B(HE) potential and the HFDHE2 and HF1MD potentials are given.

T_1 are available for ^{3}He at low temperatures, it would be worthwhile attempting an accurate *ab initio* calculation of the nuclear spin-dependent anisotropic components of the ^{3}He–^{3}He interaction.

5. Summary and conclusions

A new ground state He–He potential has been proposed in order to provide more accurate calculations of the equilibrium and nonequilibrium properties of isotopic gaseous helium over an extended temperature range (1·4 K to 2200 K). Recent *ab initio* values of the short-range (1 a.u. to 3 a.u.) repulsion energies have been taken into account in the determination of the new potential by pinning the repulsive wall at 1 a.u. to the value obtained there by Ceperly and Partridge [24]. In addition, the present potential has also been fitted to the shear viscosity [37] at 298·15 K, the second virial coefficient of ^{3}He [27] at 1·47 K, and the second virial coefficient of ^{4}He [28] at 2·60 K. It has then been tested against a large number of additional experimental data. Good quantitative agreement has been found with all reliable measurements of second virial coefficients [7, 27–29, 49, 69–71], shear viscosity [33, 36, 37, 73, 74] and thermal conductivity coefficients [34–36], both for ^{3}He and ^{4}He. Additionally, good quantitative agreement has been obtained with differential [14, 43] and integral [20] scattering data and with low temperature nuclear spin relaxation measurements [68] in ^{3}He.

Determination of a new potential for ground state He has been undertaken because the previous HFDHE2 potential of Aziz *et al.* [6], although the best yet

available, has been found to be slightly deficient for the calculation of highly precise low temperature ^{3}He and ^{4}He second virial coefficients and the transport properties at high temperatures. For example, the HFDHE2 potential predicts a $B(T)$ value for ^{4}He at 2·6 K which differs by 3 $cm^3\,mol^{-1}$ from the most accurate available experimental value [28], lying outside the error bars ($\pm 1\,cm^3\,mol^{-1}$) and a $B(T)$ value for ^{3}He at 1·47 K which differs by 4 $cm^3\,mol^{-1}$ from the most accurate available experimental value [27], also lying outside the experimental error bars ($\pm 0{\cdot}5\,cm^3\,mol^{-1}$).

Although it is difficult to interpret any comparison between the individual parameter values determining the two (slightly different) potential forms, a comparison of the depth and location of the potential well and the value at which the potentials become zero is significant. The present HFD–B(HE) potential has its minimum at $\varepsilon/k = 10{\cdot}95$ K, $r_m = 2{\cdot}963$ A while the HFDHE2 potential has its minimum at $\varepsilon/k = 10{\cdot}80$ K, $r_m = 2{\cdot}967$ A, so that the new potential is slightly deeper with the bowl shifted slightly inwards with respect to the HFDHE2 potential. The corresponding σ values are σ(HFD–B(HE)) = 2·637 A and σ(HFDHE2) = 2·639 A. These values are consistent with the improved agreement with the low temperature virial coefficient measurements, since the low temperature virial coefficient is largely sensitive to the shape and volume of the potential well. The HFDHE2 potential was also in strong disagreement with the *ab initio* repulsion energies obtained by Ceperley and Partridge [24], being of the order of 80 per cent too high over much of the domain of the calculations (1·0 a.u. to 3·0 a.u.). It is the overestimate of the repulsive wall that accounts for the incorrect prediction of the high temperature transport coefficients by the HFDHE2 potential.

This research was supported in part by grants in aid of research (R.A.A. and F.R.W.M.) from the National Science and Engineering Research Council of Canada. The authors would like to thank Dr. Alec Janzen, who assisted with the integral cross section calculations, M. F. Slaman, who helped in coding some of the preliminary computer programs, Professor R. J. Le Roy for guidance in the use of his phase shift-time delay code, and Prof. W.-K. Liu for helpful discussions regarding our DWBA calculations of the ^{3}He nuclear spin relaxation times. They would also like to acknowledge many helpful discussions with Dr. G. T. McConville, who also kindly supplied virial data prior to publication, and Drs. P. P. M. Steur, M. Moldover, J. C. Holste, K. R. Hall and E. Whalley for help in the assessment of the virial data.

References

[1] Scoles, G., 1980, *A. Rev. phys. Chem.*, **31**, 81.
[2] Ahlrichs, R. A., Penco, R., and Scoles, G., 1977, *Chem. Phys.*, **19**, 119.
[3] Tang, K. T., and Toennies, J. P., 1984, *J. chem. Phys.*, **80**, 3726.
[4] Ng, K. C., Meath, W. J., and Allnatt, A. R., 1979, *Molec. Phys.*, **37**, 237.
[5] Pack, R. T., Valentini, J. J., Becker, C. H., Buss, R. J., and Lee, Y. T., 1982, *J. chem. Phys.*, **77**, 5475. Aziz, R. A., 1984, *Inert Gases, Potentials, Dynamics and Energy Transfer in Doped Crystals*, edited by M. L. Klein (Springer-Verlag), p. 5.
[6] Aziz, R. A., Nain, V. P. S., Carley, J. S., Taylor, W. L., and McConville, G. T., 1979, *J. chem. Phys.*, **70**, 4330.
[7] Gammon, B. E., 1976, *J. chem. Phys.*, **64**, 2556.
[8] Jody, B. J., Saxena, S. C., Nain, V. P. S., and Aziz, R. A., 1977, *Chem. Phys.*, **22**, 53.
[9] Maitland, G. C., and Smith, E. B., 1972, *J. chem. Engng Data*, **17**, 150.
[10] McLaughlin, D. R., and Schaefer, H. F., III, 1971, *Chem. Phys. Lett.*, **12**, 244.

[11] GLOVER, R. M., and WEINHOLD, F., 1977, *J. chem. Phys.*, **66,** 191.
[12] UANG, Y. H., and STWALLEY, W. C., 1982, *J. chem. Phys.*, **76,** 5069.
[13] BECKER, E. W., MISENTA, R., and SCHMEISSNER, E., 1954, *Z. Phys.*, **137,** 126. BECKER, E. W., and MISENTA, R., 1955, *Z. Phys.*, **140,** 535.
[14] BURGMANS, A. L. J., FARRAR, J. M., and LEE, Y. T., 1976, *J. chem. Phys.*, **64,** 1345.
[15] KALOS, M. H., LEE, M. A., WHITLOCK, P. A., and CHESTER, G. V., 1981, *Phys. Rev.* B, **24,** 115.
[16] BECK, D. E., 1968, *Molec. Phys.*, **14,** 311; 1968, *Ibid.*, **15,** 332. BECK, D. E., 1969, *J. chem. Phys.*, **50,** 541.
[17] BRUCH, L. W., and MCGEE, I. J., 1967, *J. chem. Phys.*, **46,** 2959; 1970, *Ibid.*, **52,** 5884.
[18] DOUKETIS, C., SCOLES, G., MARCHETTI, M. ZEN, M., and THAKKAR, A. J., 1982, *J. chem. Phys.*, **76,** 3057.
[19] TANG, K. T., and TOENNIES, J. P., 1986, *Z. Phys.* D, **1,** 91.
[20] FELTGEN, R., KRIST, H., KOHLER, K. A., PAULY, H., and TORELLO, F., 1982, *J. chem. Phys.*, **76,** 2360.
[21] BURTON, P. G., 1979, *J. chem. Phys.*, **70,** 3112.
[22] LIU, B., and MACLEAN, A. D., as cited in [20].
[23] FOREMAN, P. B., ROL, P. K., and COFFIN, K. P., 1974, *J. chem. Phys.*, **61,** 1658.
[24] CEPERLEY, D. M., and PARTRIDGE, H. J., 1986, *J. chem. Phys.*, **84,** 820.
[25] STEBBINGS, R. F. (private communication).
[26] KALOS, M. H., and WHITLOCK, P. A. (private communication).
[27] MATACOTTA, F. C., MCCONVILLE, G. T., STEUR, P. P. M., and DURIEUX, M., 1987, *Metrologia* (to be published).
[28] BERRY, K. H., 1987 (private communication).
[29] GUGAN, D., 1982, *Temperature: Its Measurement and Control in Science and Industry* (American Institute of Physics), p. 33.
[30] PLUMB, H. H., 1982, *Temperature: Its Measurement and Control in Science and Industry* (American Institute of Physics), p. 77.
[31] KEMP, R. C., BESLEY, L. M., and KEMO, W. R. G., 1982, *Temperature: Its Measurement and Control in Science and Industry* (American Institute of Physics), p. 33.
[32] THAKKAR, A., 1981, *J. chem. Phys.*, **75,** 4496. KOIDE, A., MEATH, W. J., and ALLNATT, A. R., 1982, *J. phys. Chem.*, **86,** 1222.
[33] VOGEL, E., 1984, *Ber. Bunsenges. phys. Chem.*, **88,** 997.
[34] ACTON, A., and KELLNER, K., 1977, *Physica* B, **90,** 192.
[35] ASSAEL, M. J., DIX, M., LUCAS, A., and WAKEHAM, W. A., 1981, *J. chem. Soc. Faraday Trans. I*, **77,** 439.
[36] KESTIN, J., PAUL, R., CLIFFORD, A. A., and WAKEHAM, W. A., 1980, *Physica* A, **100,** 349.
[37] VOGEL, E., 1984, *Z. Wilhelm-Pieck-Universitaet, Rostock*, **33,** 34.
[38] MCCONVILLE, G. T., 1984, *Proc. 17th Int. Conf. Low Temperature Physics* (North-Holland), 401.
[39] STEUR, P. P. M., 1983, Doctoral Thesis, University of Leiden.
[40] MOLDOVER, M. R. (private communication)
[41] MEATH, W. J., and AZIZ, R. A., 1984, *Molec. Phys.*, **52,** 225.
[42] MEYER, W., as cited in [20].
[43] FARRAR, J. M., and LEE, Y. T., 1972, *J. chem. Phys.*, **56,** 5801.
[44] AUFM KAMPE, W., OATES, D. E., SCHRADER, W., and BENNEWITZ, W. G., 1973, *Chem. Phys. Lett.*, **18,** 323.
[45] FELTGEN, R., PAULY, H., TORELLO, F., and VEHMEYER, H., 1973, *Phys. Rev. Lett.*, **30,** 820.
[46] AZIZ, R. A., and CHEN, H. H., 1977, *J. chem. Phys.*, **67,** 5719.
[47] AZIZ, R. A., and SLAMAN, M. J., 1986, *Molec. Phys.*, **58,** 679.
[48] WAXMAN, M., and DAVIS, H., 1978, *J. Res. natn. Bur. Stand.*, **83,** 415.
[49] KELL, G. S., MCLAURIN, G. E., and WHALLEY, E., 1978, *J. chem. Phys.*, **68,** 2199.
[50] HOLSTE, J. C., WATSON, M. Q., BELLOMY, M. T., EUBANK, P. T., and HALL, K. R., 1980, *A.I.Ch.E. Jl*, **26,** 954.
[51] WAXMAN, M., as cited in GUILDNER, L. A., and EDSINGER, R. E., 1976, *J. Res. natn. Bur. Stand.*, **80,** 703.
[52] AZIZ, R. A., MEATH, W. J., and ALLNATT, A. R., 1983, *Chem. Phys.*, **78,** 295; 1983, *Ibid.*, 1984, *Ibid.*, **85,** 491.

[53] AZIZ, R. A., and SLAMAN, M. J., 1986, *Molec. Phys.*, **57**, 825.
[54] KILPATRICK, J. E., KELLER, W. E., HAMMEL, E. F., and METROPOLIS, N., 1954, *Phys. Rev.*, **94**, 1103.
[55] HIRSCHFELDER, J. O., CURTISS, C. F., and BIRD, R. B., 1954, *Molecular Theory of Gases and Liquids* (Wiley), Chap. 6.
[56] MASON, E. A., and SPURLING, T. H., 1969, *The Virial Equation of State*, Vol. 10/2, edited by J. H. Rowlinson (Pergamon Press).
[57] ROMAN, P., 1965, *Advanced Quantum Theory* (Addison-Wesley), p. 489.
[58] CLENSHAW, C. W., and CURTIS, A. R., 1960, *Num. Math.*, **2**, 197.
[59] O'HARA, H., and SMITH, F. J., 1971, *Comput. Phys. Commun.*, **2**, 47; 1971, *Ibid.*, **3**, 173. NEUFELD, P. D., and AZIZ, R. A., 1972, *Comput. Phys. Commun.*, **3**, 269. PRICE, S. L., 1980, *Comput. Phys. Commun.*, **19**, 271.
[60] MUNN, R. J., SMITH, F. J., MASON, E. A., and MONCHICK, L., 1965, *J. chem. Phys.*, **42**, 537. IMAM-RAHAJOE, S., CURTISS, C. F., and BERNSTEIN, R. B., 1965, *J. chem. Phys.*, **42**, 530.
[61] MONCHICK, L., MASON, E. A., MUNN, R. J., and SMITH, F. J., 1965, *Phys. Rev.*, **139**, A1076.
[62] LE ROY, R. J., 1979, Computer program for calculating phase shifts and time delays for scattering on a spherical potential, CP-107R (University of Waterloo Chemical Physics Report, Waterloo).
[63] Ref. [55], pp. 604, 605.
[64] CHAPMAN, R., and RICHARDS, M. G., 1974, *Phys. Rev. Lett.*, **33**, 18.
[65] ABRAGAM, A., 1961, *Principles of Nuclear Magnetism* (Oxford University Press), Chap. 8.
[66] CHEN, F. M., and SNIDER, R. F., 1967, *J. chem. Phys.*, **46**, 3939.
[67] SHIZGAL, B., 1970, *J. chem. Phys.*, **58**, 3424.
[68] CHAPMAN, R., 1976, *Phys. Rev.* A, **12**, 2333.
[69] STEUR, P. P. M., DURIEUX, M., and MCCONVILLE, G. T., 1987, *Metrologia* (in the press).
[70] KEMP, R. C., KEMP, W. R. G., BESLEY, L. M., 1987, *Metrologia*, **23**, 61.
[71] MCCONVILLE, G. T. (private communication).
[72] CAMERON, J. A., and SEIDEL, G. M., 1985, *J. chem. Phys.*, **83**, 3621.
[73] CLARKE, A. G., and SMITH, E. B., 1968, *J. chem. Phys.*, **48**, 3988; 1969, *Ibid.*, **51**, 4156.
[74] GUEVARA, F. A., MCINTEER, B. B., and WAGEMAN, W. E., 1969, *J. chem. Phys.*, **12**, 2493.
[75] GUEVARA, F. A., STENSLAND, G., 1971, *Phys. Fluids*, **14**, 746.
[76] GOLDBLATT, M., GUEVARA, F. A., and MCINTEER, B. B., 1970, *Phys. Fluids*, **13**, 2873.
[77] HAARMAN, J. W., 1973, *A.I.P. Conf. Proc. No. 11*, p. 193.
[78] AZIZ, R. A., and VAN DALEN, A., 1983, *J. chem. Phys.*, **78**, 2402.
[79] SHIZGAL, B., 1973, *Chem. Phys. Lett.*, **20**, 265.